High-Temperature Materials

SCIEPublish

Article

# Transformation Characteristics of Gucheng Quartzite and Assessment of Its Application Prospects

**Qian Xu [1], Bing Fan [1,2,3,*], Defeng Zhang [4], Yucheng Yin [1,2,*] and Shengli Jin [1,2]**

[1] State Key Laboratory of Advanced Refractories, Wuhan University of Science and Technology, Wuhan 430081, China; xuqian336688@163.com (Q.X.); shengli.jin@wust.edu.cn (S.J.)
[2] Joint International Research Laboratory of Refractories and Metallurgy, Wuhan University of Science and Technology, Wuhan 430081, China
[3] Huayi New Materials (Xiangyang) Co., Ltd., Xiangyang 441721, China
[4] Yancheng Institute of Technology, School of Automotive Engineering, Yancheng 224051, China; dez@ycit.edu.cn (D.Z.)

* Corresponding author. E-mail: fanbing@huayinm.com.cn (B.F.); yinyucheng@wust.edu.cn (Y.Y.)

Received: 20 July 2026; Revised: 13 August 2026; Accepted: 7 September 2026; Available online: 17 September 2026

**ABSTRACT:** With the aim to well understand the relationship between the composition and properties of quartzite in Gucheng, three types of quartzite from a mining area in Gucheng have been investigated. This paper focused on the phase composition evolution and thermal expansion behavior of them under different thermal histories in the temperature range of 1200 °C to 1500 °C, and subsequently, the true density and microstructure were also measured and analyzed. In addition, inclusion analysis was conducted. The results indicate that black quartzite has a higher Fe content, white quartzite has relatively higher Al and K contents, and gray quartzite has a higher Ca content. Furthermore, all three types of quartzite almost completely transform into cristobalite after heat treatment at 1500 °C, although the transformation rates vary slightly with increasing temperature. The thermal expansion of the three types of quartzite exhibits similar trends, but gray quartzite exhibits greater residual expansion. It is believed that the phase transformation plays a dominant role in the total expansion, together with the sintering effect accelerated by the glass phase. At the same time, the microstructure of quartzite was also significantly influenced by the phase transformation process. The gas/liquid inclusion analysis revealed that all three types of quartzite have high inclusion content. The black quartzite contained only 5% transparent particles, the lowest among the three specimens, none of the three quartzite types are suitable for direct use in high-purity quartz applications.

**Keywords:** Quartz; Phase composition; Microstructure; Gas/liquid inclusions

## 1. Introduction

Quartzite is a naturally occurring rock composed mainly of quartz [1]. It serves as a vital raw material for modern industry, particularly in the building materials, metallurgy, chemical, and high-tech sectors, and holds immense technological significance [2–5], which depends heavily on the types and concentrations of impurities in quartzite. The impurities existing as inclusions make the purification of quartzite more difficult, thereby limiting its scope of application [6].

Quartzite in Gucheng, China, is characterized by two key features, large reserves and a high concentration of $SiO_2$. The cumulative proven reserves of quartzite in Gucheng amount to 62.28 million tons, with potential reserves reaching 200 million tons, providing ample raw material for the development of China's silicon-based materials industry. The average $SiO_2$ content in Gucheng quartzite exceeds 99.5 wt% [7], which is ranked one of the highest-quality domestic mineral products of its kind and is particularly suitable for the production of high-tech products such as polycrystalline silicon and monocrystalline silicon. Currently, Gucheng quartzite is primarily used as a metallurgical raw material in the polysilicon and monocrystalline silicon industries, as well as for applications such as high-purity silicon micro-powder [8].

Gucheng quartzite is predominantly gray, though it also contains small amounts of black and white ore. To develop more high-end applications for Gucheng quartzite, mechanical color sorting and grading have become essential, and this technology is gradually being adopted. It is well known that the color of mineral ores is closely related to their chemical compositions. The correlation between ore colour and specific impurity elements can be explained mechanistically in terms of the valence state and mode of occurrence of each impurity, rather than simply by its bulk concentration. Iron is the dominant chromophore in these rocks. In natural quartz, Fe occurs either as $Fe^{3+}$ substituting for $Si^{4+}$ in tetrahedral sites or as fine-grained iron-oxide inclusions, tetrahedrally coordinated $Fe^{3+}$ absorbs visible light through d–d transitions and ligand-to-metal charge-transfer (LMCT) transitions, imparting dark to reddish-brown tones, whereas isolated $Fe^{2+}$ tends to produce a greenish tint. The black colour of the Fe-rich ore therefore indicates that Fe is present mainly as $Fe^{3+}$, most plausibly coexisting with $Fe^{2+}$ in a mixed-valence state (e.g., magnetite-type inclusions) or as abundant opaque iron-oxide inclusions, both of which give rise to strong absorption across the entire visible range [9]. By contrast, $Al^{3+}$ and $K^{+}$ enter the quartz lattice as the charge-compensated substitution pair $[AlO_4/K^{+}]^0$ [10]. Because this defect contains no transition-metal d electrons, it does not absorb visible light, so the ore remains white or colorless, its whiteness therefore reflects the near-absence of Fe chromophore centers rather than the Al and K themselves. The gray color of the Ca-rich ore does not arise from electronic absorption: the $Ca^{2+}$ ionic radius is too large for it to substitute for $Si^{4+}$, so Ca is instead hosted in Ca-bearing fluid inclusions and micro-mineral inclusions. The high abundance of these inclusions induces light scattering (Tyndall scattering), producing the milky-gray appearance [11,12].

However, the relationship between quartzite color and its composition and phase transformations has not yet received sufficient attention. Therefore, this paper aims to investigate the relationship between the color of quartz from a specific lode in Gucheng and its composition, while clarifying its heating transformation process and thermal expansion behavior, and characterizing its inclusions, in order to provide a theoretical basis and technical guidance for extending the applications of Gucheng's quartzite.

## 2. Materials

The quartzite used in this paper includes three colors, black, white, and gray—from a mining area in Gucheng, as shown in Figure 1. Quartzite in different are labeled as Silica B (black), Silica W (white), and Silica G (gray), respectively. The chemical compositions of them are shown in Table 1.


**Figure 1.** Appearance of quartzite, (**a**) Silica B, (**b**) Silica W, (**c**) Silica G.

**Table 1.** Chemical composition of three quartz samples, wt%.

| | $SiO_2$ | $Al_2O_3$ | $Fe_2O_3$ | $TiO_2$ | CaO | MgO | $K_2O$ | $Na_2O$ | MnO | $B_2O_3$ |
|---|---|---|---|---|---|---|---|---|---|---|
| Silica B | 99.51 | 0.039 | 0.260 | 0.005 | 0.003 | 0.023 | 0.005 | 0.001 | 0.033 | 0.004 |
| Silica W | 99.65 | 0.100 | 0.003 | 0.004 | 0.077 | 0.012 | 0.070 | 0.012 | 0.014 | 0.001 |
| Silica G | 99.69 | 0.082 | 0.050 | 0.002 | 0.130 | 0.006 | 0.005 | 0.008 | 0.023 | 0.001 |

As shown in Table 1, the main component, $SiO_2$, in all three types of quartzite is greater than 99.5 wt%. A comparison reveals that the $Fe_2O_3$ content in Silica B reaches 0.26 wt%, which is significantly higher than that of the other two quartzite samples. In Silica W, the $Al_2O_3$ and $K_2O$ contents are notably higher than those of the other two, reaching 0.10 wt% and 0.07 wt%, respectively. Silica G has the highest CaO content of 0.13 wt%.

The fracture microstructures of the three types of quartzite are shown in Figure 2. Their crystal grain size was analyzed according to Figure 3, and the results are shown in Figure 3. As can be seen in Figures 2a and 3a, the fracture surface of Silica B is a fracture surface free of fine adhering particles, with grain sizes primarily ranging from 4 to 14 μm and an average grain size of 10.1 μm. Figures 2b and 3b show that the grain size of Silica W is primarily distributed between 2 and 14 μm, with an average grain size of 7.2 μm, fine and flaky crystals can be observed in its fracture surface. The quartz grains in this sample are noticeably smaller than those in Silica B. Figures 2c and 3c show that the fracture surface of Silica G is relatively fracture surface free of fine adhering particles, with grain sizes primarily ranging from 2 to 14 μm and an average grain size of 8.2 μm.

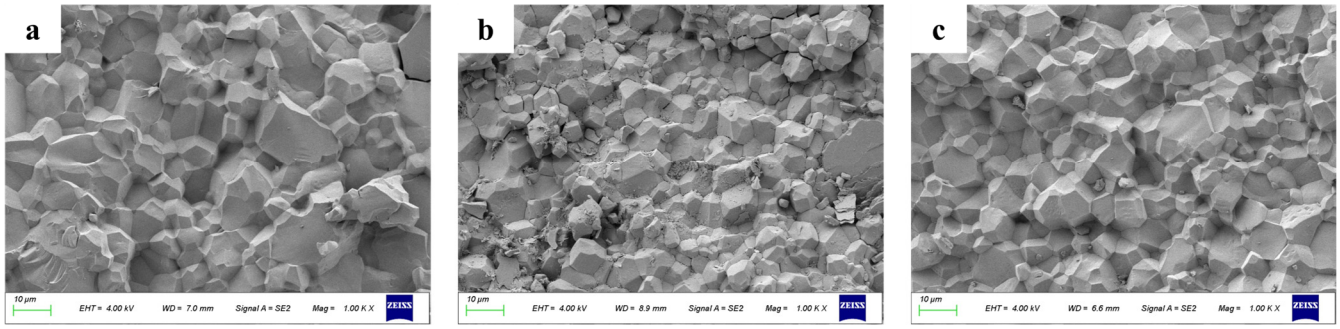


**Figure 2.** Morphology of fractured quartzite samples, (**a**) Silica B, (**b**) Silica W, (**c**) Silica G.

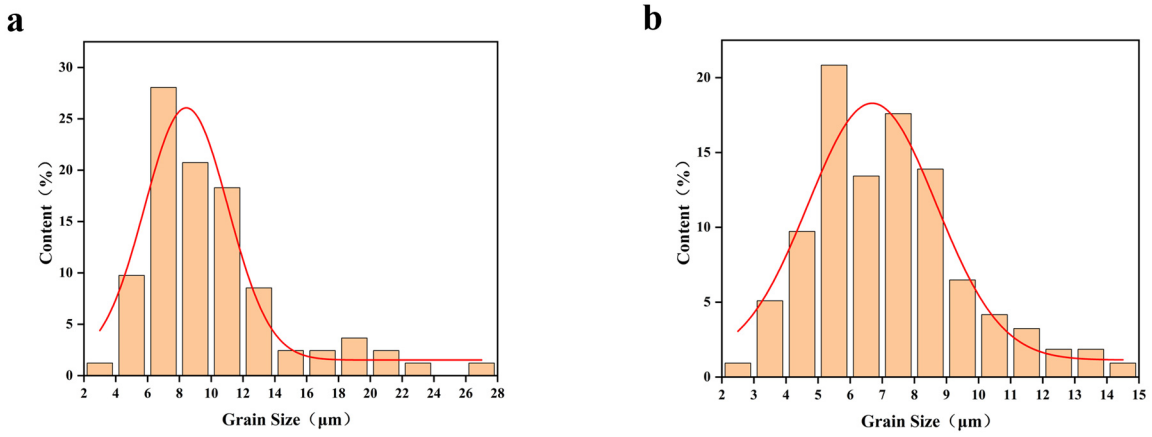

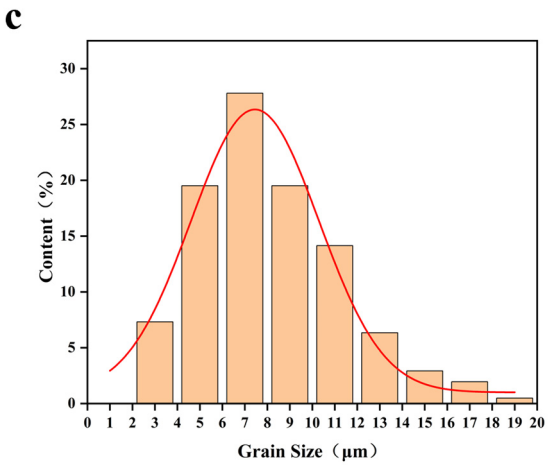


**Figure 3.** Grain size distribution of the quartzite, (**a**) Silica B, (**b**) Silica W, (**c**) Silica G.

## 3. Methodology

The significant irreversible quartz-to-cristobalite transformation occurs above approximately 1200 °C. The sintering temperature of silica refractory products is usually around 1400 °C. In contrast, the α-β quartz transition at 573 °C is reversible and rapid, and it has already been reflected in the thermal expansion tests. Therefore, the phase composition study was focused on the temperature range of 1200–1500 °C.

In order to compare the microstructure difference before and after heat treatment, quartzite samples were cut into 10 mm × 5 mm × 5 mm rectangular specimens for heat treatment. Powder finer less 200 mesh has been prepared by crushing to meet the XRD and XRF analysis. 10 mm × 5 mm × 5 mm rectangular specimens and powder less than 200 mesh were calcined at 1200 °C, 1300 °C, 1400 °C, and 1500 °C [13] for 3 h in a muffle furnace (KF1600, Nanjing Boyuntong Instrument Technology Co., Ltd., Nanjing, China), respectively. Afterward, the phase composition of the powder was analyzed by XRD, and the true density was measured using a gas pycnometer (Micromeritics AccuPyc 1330, Micromeritics Instrument Corporation, Norcross, GA, USA) according to ASTM C604-18 [14]. Microstructural analysis and elemental composition were performed on rectangular specimens by SEM (ZEISS Gemini SEM 560, Carl Zeiss Microscopy GmbH, Jena, Germany) to identify the phase transformation induced microstructure evolution.

The thermal expansion of the three types of quartzite was determined according to ISO 16835:2014 [15] push rod method during a heating-cooling cycle ranging from room temperature to 1500 °C. Inclusions in the different types of quartzite were statistically analyzed using an optical microscope.

## 4. Results and Discussion

### *4.1. Mineral Transformation Processes*

The XRD patterns of the original quartzite and after heat treatment at different temperatures are shown in Figure 4. It can be seen that the main mineral composition of all three types of silica was quartz after heat treatment at 1200 °C, although characteristic diffraction peaks of cristobalite began to appear. As the temperature increased further to 1300–1400 °C, the characteristic diffraction peaks of cristobalite intensified significantly, while the diffraction intensity of quartz continued to decrease, indicating that quartz was continuously transforming into cristobalite. When the temperature reached 1500 °C, quartz almost completely transformed into cristobalite; only a small amount of the quartz phase could be detected in the XRD patterns. Overall, the three types of quartzite exhibited a similar heating transformation process. The XRD results of the samples were semi-quantitatively analyzed by refinement using HighScore Plus software, and the results are shown in Table 2.

**Table 2.** Cristobalite content at different temperatures, wt%.

| Sample | 1200 °C | 1300 °C | 1400 °C | 1500 °C |
|---|---|---|---|---|
| Silica B | 10.3 | 19.4 | 52.9 | 90.7 |
| Silica W | 8.2 | 19.8 | 48.6 | 91.5 |
| Silica G | 7.1 | 22.8 | 49.1 | 93.2 |

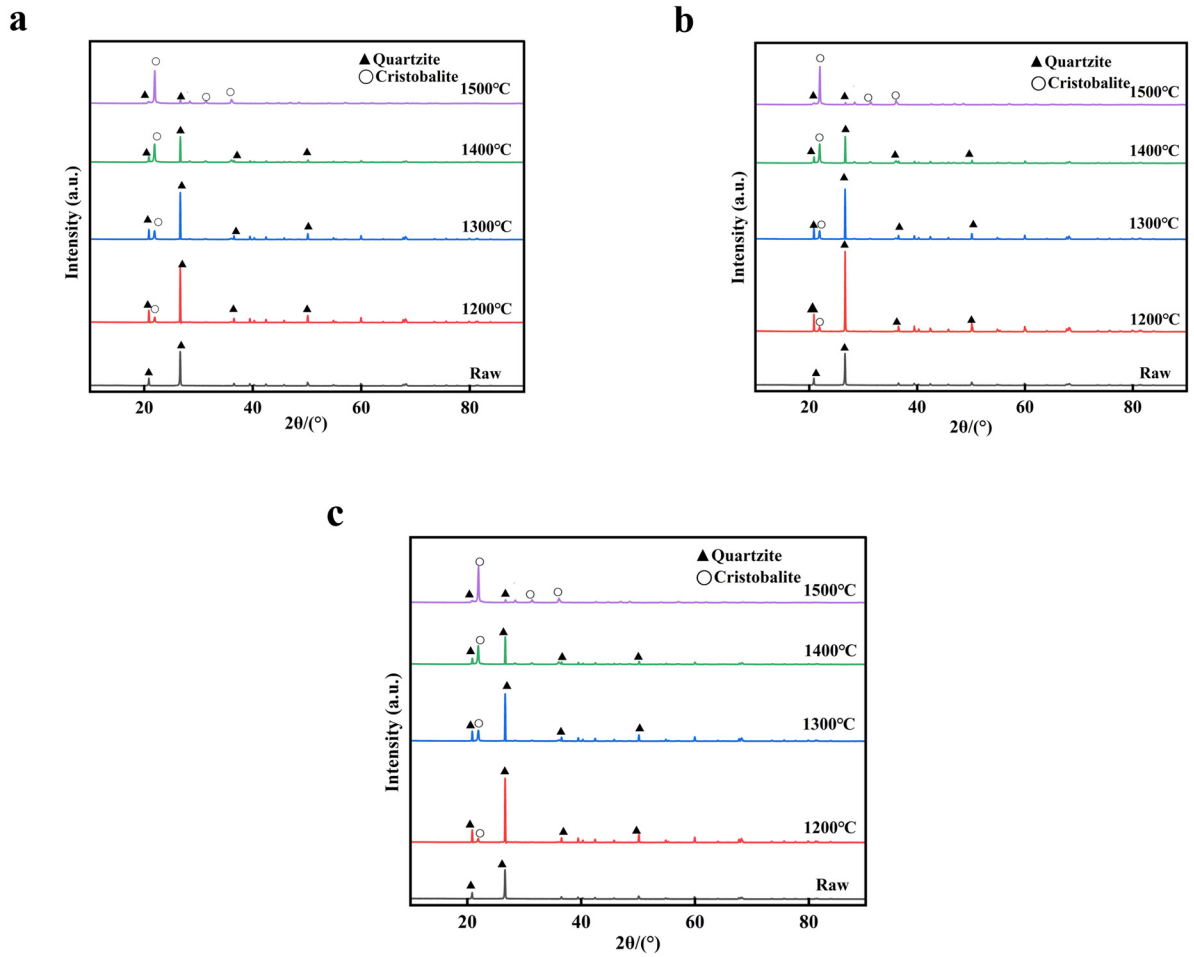


**Figure 4.** XRD patterns of three types of quartzite after heat treatment, (**a**) Silica B, (**b**) Silica W, (**c**) Silica G.

True density measurements were carried out, and the results are presented in Figure 5. The true density decreased as the heat treatment temperature increased within the temperature range of 1200 °C to 1500 °C. This is primarily due to the phase transition from quartz ($\rho$ = 2.65 g/cm$^3$) to cristobalite ($\rho_c$ = 2.32 g/cm$^3$). The theoretical density values of the two $SiO_2$ polymorphs were taken from the standard data of Heaney [16]. Additionally, it can be observed that Silica W exhibited the greatest decrease in true density at 1200 °C, suggesting a faster transformation rate. When the heat treatment temperature was in the range of 1300 °C–1400 °C, Silica W exhibited the lowest true density, which indicates that its transformation rate exceeds that of the other two quartzite samples. However, as the temperature increased to 1500 °C, all three quartzite samples had essentially completed the transformation from quartz to cristobalite, and the differences in true density among them had also narrowed compared to earlier stages.

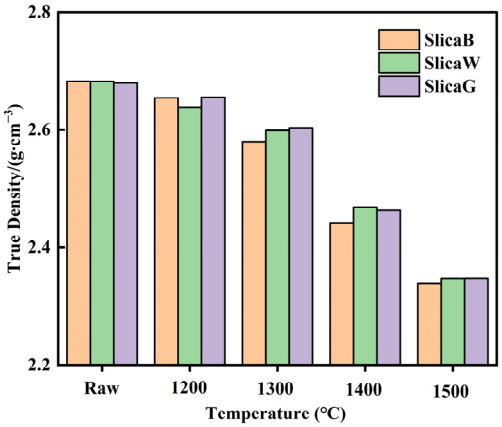


**Figure 5.** True Density of Test Specimens VS Calcination Temperature.

Overall, as shown in Figure 6, at 1200 °C, Silica B exhibited a faster transformation rate, while in the 1300 °C range, Silica G's transformation rate was higher than that of the other two samples. When the temperature rose to 1500 °C, among the three quartzites, Silica G exhibited the highest conversion rate, at 93.2%. The transformation of all three quartzites was almost complete [17], and the three quartzites achieved conversion rates above 90%, as shown in Table 2.

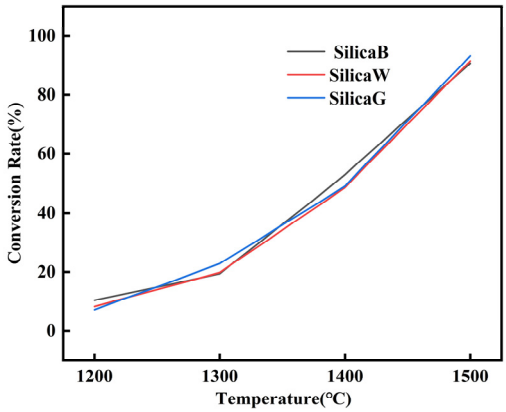


**Figure 6.** Conversion rate of quartz into cristobalite at different temperatures.

### *4.2. Microstructural Evolution*

The microstructures of the quartzite after heat treatment at different temperatures are shown in Figure 7. It can be seen that as the heat treatment temperature increases, the morphology of the three types of quartzite undergoes significant changes. As quartz transforms into cristobalite, the number of pores in the specimen surface increases, and a small number of cracks form. At 1300 °C, slight cracks appear on the surface of Silica B, indicating that the transformation of the quartzite appears to begin at this temperature. As the temperature rises, the number of cracks on the surfaces of the three quartzite gradually increases, and at 1500 °C, a large number of distinct cracks appear, indicating that the quartz phase in the quartzite has almost completely transformed into the cristobalite phase. As shown in the microstructure and grain size distribution of Silica B in Figures 8 and 9, the grain size sometimes increases as the temperature rises, to 1500 °C due to high-temperature liquid-phase precipitation. Meanwhile, the grain shape cannot be clearly observed, and desiccation-like cracks appear. The quantitative results in Table 2 also show a significant

increase in cristobalite content at 1300–1400 °C, consistent with the cracking caused by volume expansion observed in Figure 7.

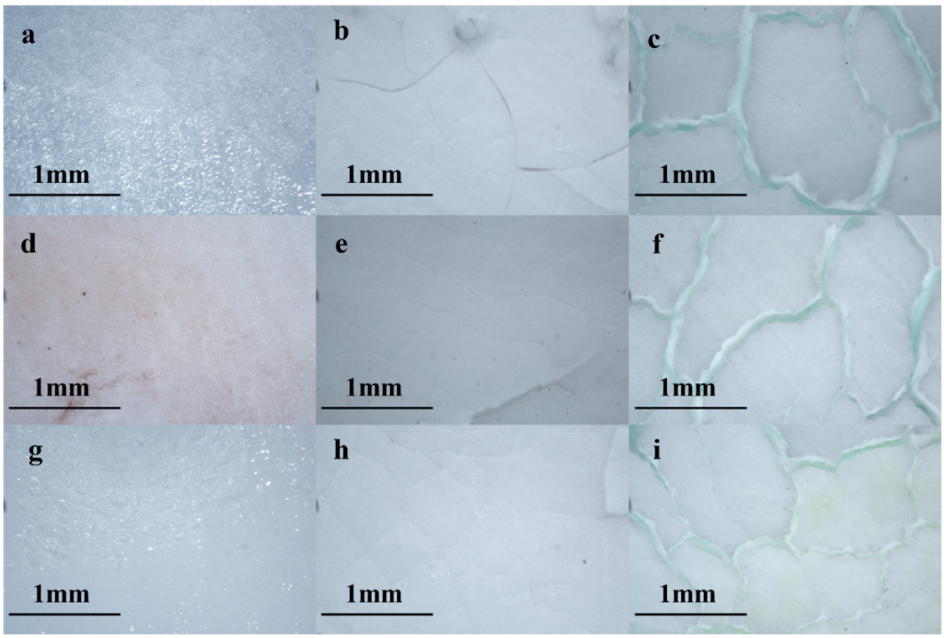


**Figure 7.** Macro Structure of quartzite after heat treatment, (**a**), (**b**), (**c**) Silica B heat treated at 1300 °C, 1400 °C and 1500 °C, respectively, (**d**), (**e**), (**f**) Silica W heat treated at 1300 °C, 1400 °C and 1500 °C, respectively, (**g**), (**h**), (**i**) Silica G heat treated at 1300 °C, 1400 °C and 1500 °C, respectively.

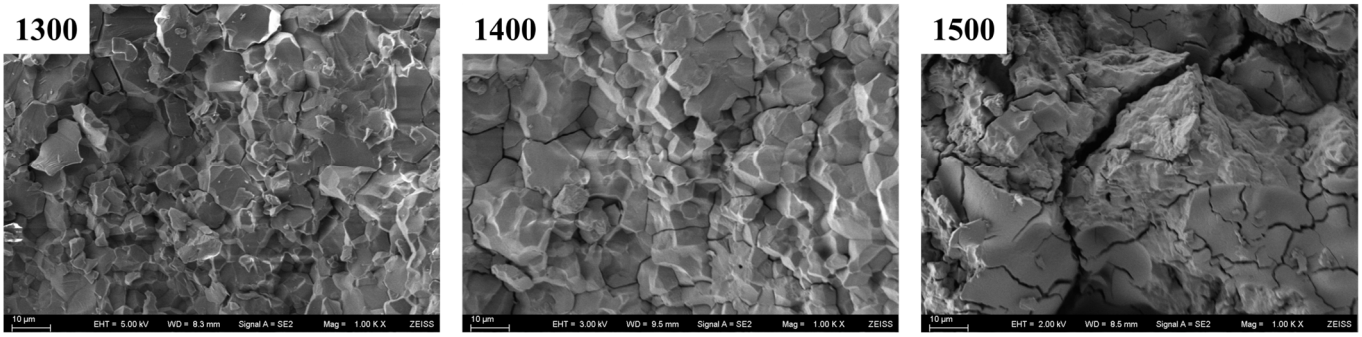


**Figure 8.** Morphology of fractured Silica G at 1300–1500 °C.

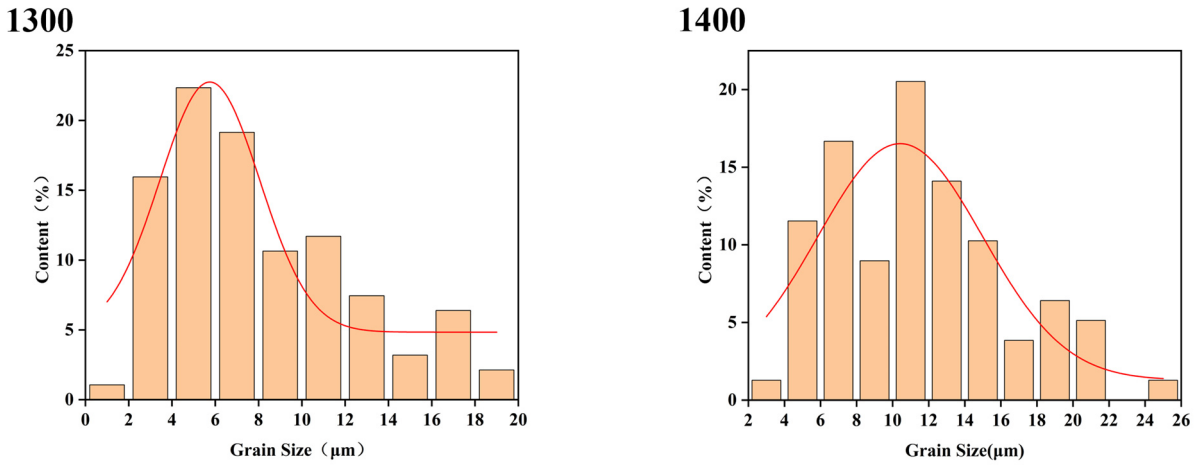


**Figure 9.** Grain size distribution of the Fracture of Silica G at 1300–1400 °C.

### *4.3. Thermal Expansion Behavior*

Figure 10 shows the thermal expansion of quartzite during a heating and cooling cycle in the temperature range of room temperature to 1500 °C. During the heating process from room temperature to 1500 °C, the three types of quartzite exhibited nearly identical thermal expansion behavior. At 573 °C, the phase transition between the α and β forms of quartz occurred [18], causing the maximum expansion of approximately 1.5% to be reached before 600 °C. When the temperature exceeded 1350 °C, the Silica B and W underwent a contraction process, which may be related to sintering shrinkage induced at high temperatures, Liquid contents of each sample at high temperature were predicted by FactSage6.4 [19]. The database used was FToxid, after normalizing the chemical composition listed in Table 1, the data obtained (shown in Table 3) were entered into FactSage for the composition simulation, the temperature range was set from 600–1500 °C, the temperature interval of 100 °C, and the pressure set was as 1 atm. The prediction of liquid contents was performed in the temperature range of 600–1500 °C with the interval of 100 °C. The results were plotted and shown in Figure 11. It can be read from Figure 11 that the liquid phase formation began at 800 °C for all of three samples. While sample W presented a quicker increase, as well as a much more temperature dependence than the other two. At the same time, sample W also contained also a highest liquid amount which will definitely influence its expansion in the temperature of 1400–1500 °C by promoting its sintering procedure, as shown in Figure 10. For samples B and G they showed a little bit higher expansion than W due to their little liquid contents correspondingly. However, sample G presented a higher expansion than B, even though it contained much more liquid phase than B. According to the semi-quantitative analysis results in Table 2, Silica G exhibits the highest quartz-to-cristobalite transformation ratio among the three samples. This leads to additional expansion in Silica G under the same conditions, making its thermal expansion ratio the largest among the three.

Combining the SEM micrographs of the fracture surface of Silica G in Figure 8 with the FactSage liquid-phase simulation results in Figure 10, it can be observed that samples heat-treated at 1300–1400 °C show no obvious microcracks. However, when the heat-treatment temperature is raised to 1500 °C, noticeable microcracks appear in the microstructure. Since the FactSage results indicate that a considerable amount of liquid phase forms at 1500 °C, the cracking is most likely attributed to the residual glass phase that solidifies from this liquid upon cooling: the thermal-expansion mismatch between the glass phase and the crystalline matrix generates tensile stress that exceeds the strength of the glass, thereby inducing microcracks.

**Table 3.** The composition (normalized mass percentages) of each component input into FactSage, wt%.

| | $SiO_2$ | $Al_2O_3$ | $Fe_2O_3$ | $TiO_2$ | CaO | MgO | $K_2O$ | $Na_2O$ | MnO | $B_2O_3$ |
|---|---|---|---|---|---|---|---|---|---|---|
| Silica B | 99.6266 | 0.0390 | 0.2603 | 0.0050 | 0.0030 | 0.0230 | 0.0050 | 0.0010 | 0.0330 | 0.0040 |
| Silica W | 99.7068 | 0.1001 | 0.0030 | 0.0040 | 0.0770 | 0.0120 | 0.0700 | 0.0120 | 0.0140 | 0.0010 |
| Silica G | 99.6930 | 0.0820 | 0.0500 | 0.0020 | 0.1300 | 0.0060 | 0.0050 | 0.0080 | 0.0230 | 0.0010 |

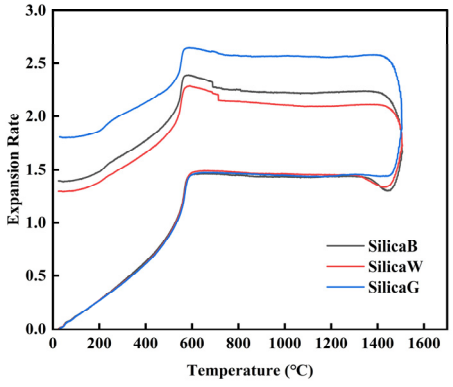


**Figure 10.** Thermal Expansion Curve of the Samples.

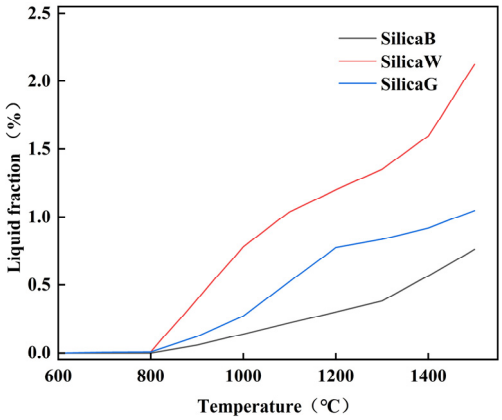


**Figure 11.** Liquid-Phase Simulation of a Sample.

During the cooling process from 1500 °C to room temperature, the thermal expansion of the three types of quartzite generally continued to increase. This is because the heating rate in the thermal expansion test was 5 °C/min, but the phase transition from quartz to cristobalite takes time, resulting in a delay in the expansion effect caused by the phase transition on the thermal expansion curve. However, there are also significant differences in the thermal expansion behavior of the three quartzite: Silica B and W are similar, while Silica G exhibits significantly greater thermal expansion. During cooling from 1500 °C to 700 °C, the expansion rate remains essentially constant (normal contraction). At around 700 °C, the expansion rate rises gradually, and this anomalous expansion persists until ~570 °C, after which the rate ceases to increase and begins to decrease. The rise at 700 °C is attributed to the continuation of the quartz-to-cristobalite transition during cooling: because this reconstructive transition is kinetically sluggish, it is incomplete on heating at 5 °C/min and proceeds further on cooling, contributing additional volume expansion. The subsequent turn-around at ~570 °C corresponds to the displacive β-quartz → α-quartz inversion of the residual β-quartz, whose contraction offsets and eventually exceeds the expansion from the continued cristobalitization, causing the expansion rate to decrease [20]. Additionally, it is worth noting that after undergoing heating-cooling cycles from room temperature to 1500 °C, all three quartzite exhibited a residual thermal expansion of approximately 1.2–1.5%, which is attributed to the irreversible phase transition from quartz to cristobalite in the quartzite.

### *4.4. Inclusion Analysis*

Inclusions refer to mineralizing fluids that are trapped and sealed within a crystal during the formation of a mineral. When the impurities consist primarily of gaseous and liquid phases, they are also referred to as gas-liquid (fluid) inclusions [21]. Among these, fluid inclusions are the most common type of inclusion formed during the growth of quartz crystals. They also include fluid inclusions formed when mineralizing fluids penetrate the fissures of already formed quartz crystals and become sealed within them (also known as secondary fluid inclusions) [22].

Methods for characterizing inclusions in quartzite primarily include optical microscopy, dual-end contrast analysis (DECA), Raman spectroscopy [23], and compositional analysis techniques [24]. Their characterization has evolved from traditional qualitative descriptions to data-driven quantitative metrics, with the proportions of permeable and impermeable particles derived from the DECA method currently serving as key evaluation criteria directly linked to the quality and application performance of high-purity quartz.

Inclusion analysis was conducted on the three types of quartzite, and the inclusions in the quartzite are shown in Figure 12. Analysis of the proportions of transparent (T) particles and non-transparent (NT) particles in the three types of quartzite is presented in Table 4. It can be seen that Silica B has the lowest T

ratio, with T ratio accounting for only 5%. However, the NT ratio in all three types of quartzite is relatively high, at around 45%.

Gas-liquid inclusions have a significant impact in fields such as high-purity quartz and photovoltaic components, while their influence is relatively minor in areas like refractory concrete and aggregates. Furthermore, according to Fan Ting [25], the evaluation of quartz gas-liquid inclusions requires a comprehensive consideration of both the proportion of transparent particles and the proportion of non-transparent particles, with the proportion of transparent particles showing a positive correlation with the quality of quartz crucibles. When the content of non-transparent in the gas-liquid inclusions within quartzite is less than 60%, the it will resulting poor transparency of quartz crucibles exhibit poor transparency, conversely, when the content of non-transparent reaches 20%, the prepared quartz crucibles contain a large number of bubbles. Therefore, none of the three types of quarzite are suitable for use in quartz crucibles. However, due to the high $SiO_2$ purity and low impurity content of the quartize, it meets the requirements for ceramics and refractory materials [26]. According to the YB/T 5268-2014 [27] standard, quartize used for silica bricks should meet the requirements of （($SiO_2 > 96\%$, $Al_2O_3 < 1.3\%$, and $Fe_2O_3 < 1.3\%$）). The quartzite investigated in this study all meet the physicochemical requirements specified in this standard for quartzite used for silica bricks, and are far superior to the minimum threshold for “refractory-grade silica” [28], and possess good high-temperature resistance, undergo relatively complete transformation at high temperatures, and have a low true density.

**Table 4.** The ratio of permeable to impermeable silica particles.

| Number | Transparent Particles | Non-Transparent |
|---|---|---|
| Silica B | 5% | 45% |
| Silica W | 14% | 43% |
| Silica G | 16% | 46% |

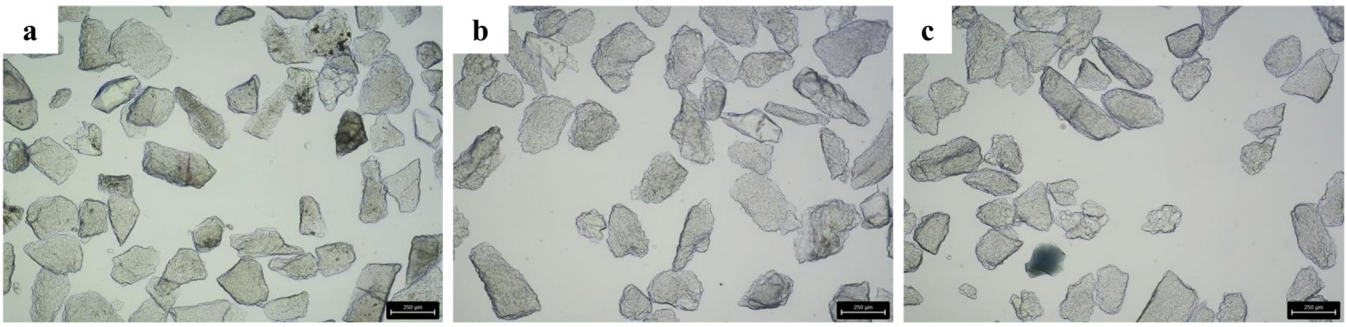


**Figure 12.** Forms of silica inclusion, (**a**) Silica B, (**b**) Silica W, (**c**) Silica G.

## 5. Conclusions

The color variation among the Gucheng quartzite primarily originates from impurity elements in the ore. The black quartize is relatively enriched in Fe, the white quartize is characterized by Al and K enrichment, and the gray quartize is distinguished by a significantly higher Ca content.

FactSage equilibrium predictions show that a liquid phase appears above ~800 °C in all three quartzites. Silica W yields the largest and most temperature-sensitive liquid fraction, thereby accelerating its transformation and sintering at 1200–1400 °C, whereas Silica G attains the highest final conversion (93 wt% cristobalite) at 1500 °C. During cooling, all three quartzite exhibit dilatometric anomalies that expansion increase gradually with the temperature down to ~700 °C, followed by a rapid decrease in expansion rate at ~570 °C due to the β→α inversion, which leaves an irreversible residual expansion of approximately 1.2–1.5%. The microstructure evolution is mainly determined by the phase transformation procedure.

Nevertheless, the glass phase contents and conversation rate of quartz into cristobalite also play a combined influence to the microstructure change.

Inclusion statistics indicated that all three quartzites could not satisfy the threshold for crucible-grade high-purity quartz production, reconciling their high bulk purity with the inclusion burden that ultimately governs high-end application performance. Nevertheless, all three ores exceed the technical limits for silica brick by a wide margin.

## Statement of the Use of Generative AI and AI-Assisted Technologies in the Writing Process

In the course of preparing this manuscript, the authors employed AI-assisted language tools exclusively for improving readability, polishing phrasing, and correcting grammatical errors. All other aspects of this work—including data collection, analysis, interpretation, figure preparation, and the formulation of scientific conclusions—were performed entirely by the authors without the involvement of any AI-based applications.

## Acknowledgments

The authors appreciate the Hua Yi new materials (Xiang Yang) company providing quartzite samples for investigation. In addition, true density and thermal expansion testing by Zhiqiang Liu from State Key Laboratory of Advanced Refractories, Wuhan University of Science and Technology were also gratefully appreciated.

## Author Contributions

Q.X.: Conceptualization, Methodology, Literature review, Writing—original draft, Review & editing. B.F.: Conceptualization, Methodology, Review and editing. D.Z.: Supervision, Review and editing. Y.Y.: Methodology, Guidance, Review and editing. S.J.: Funding acquisition, Review and editing.

## Ethics Statement

Not applicable.

## Informed Consent Statement

Not applicable.

## Data Availability Statement

Not applicable.

## Funding

The financial support from the Open Foundation of the State Key Laboratory of Advanced Refractory Materials (Wuhan) (Grant No. G202305), the High-End Foreign Experts Program (Grant No. 2022EJD021), and the Hubei Provincial Special Fund for Central-Guided Local S&T Development (Grant No. 2025CSA017) is gratefully acknowledged.

## Declaration of Competing Interest

The authors declare that they have no known competing financial interests or personal relationships that could have appeared to influence the work reported in this paper.

## References

1. Flörke OW, Graetsch HA, Brunk F, Benda L, Paschen S, Bergna HE, et al. Silica. In *Ullmann's Encyclopedia of Industrial Chemistry*; Wiley-VCH GmbH: Weinheim, Germany, 2000. DOI:10.1002/14356007.a23_583

2. Walther, Hartmut B. Quality requirements of quartz sand in the building industry. In *Quartz: Deposits, Mineralogy and Analytics*; Springer: Berlin/Heidelberg, Germany, 2012; pp. 53–70. DOI:10.1007/978-3-642-22161-3_3
3. Long H, Zhu D, Pan J, Li S, Yang C, Guo Z. Advanced processing techniques and impurity management for high-purity quartz in diverse industrial applications. *Minerals* **2024**, *14*, 571. DOI:10.3390/min14060571
4. Hu QY, Shu JF, Yang WG, Park C, Chen MW, Fujita T, et al. Stability limits and transformation pathways of α-quartz under high pressure. *Phys. Rev. B* **2017**, *95*, 104112. DOI:10.1103/PhysRevB.95.104112
5. Vatalis KI, Charalambides G, Benetis NP. Market of high purity quartz innovative applications. *Procedia Econ. Financ.* **2015**, *24*, 734–742. DOI:10.1016/S2212-5671(15)00688-7
6. Zhang R, Tang C, Ni W, Yuan J, Zhou Y, Liu X. Research Status and Challenges of High-Purity Quartz Processing Technology from a Mineralogical Perspective in China. *Minerals* **2023**, *13*, 1505. DOI:10.3390/min13121505
7. Du S, Pan B, Xia L, Zhu G, Wu L, Yu C, et al. Purification of Vein Quartz Using a New Fluorine-Free Flotation: A Case from Southern Anhui Province, China. *Minerals* **2024**, *14*, 1191. DOI:10.3390/min14121191
8. Zhu B. Evaluation of Silicon Ore Resource Exploration and Sustainable Development Strategy. *China Resour. Compr. Util.* **2024**, *42*, 114–116. DOI:10.3969/j.issn.1008-9500.2024.08.030
9. Rossman GR. Colored varieties of the silica minerals. *Rev. Mineral. Geochem.* **1994**, *29*, 433–467. DOI:10.1515/9781501509698-018
10. Dennen WH. Stoichiometric substitution in natural quartz. *Geochim. et Cosmochim. Acta* **1966**, *30*, 1235–1241. DOI:10.1016/0016-7037(66)90122-0
11. Götze J. Chemistry, textures and physical properties of quartz—Geological interpretation and technical application. *Mineral. Mag.* **2009**, *73*, 645–671. DOI:10.1180/minmag.2009.073.4.645
12. Roedder E. Fluid inclusions. In *Reviews in Mineralogy*; Mineralogical Society of America: Chantilly, VA, USA, 1984; Volume 12, pp. 1–644.
13. Fan B, Peng CL, Long SL, Li QX, Cheng W, Wang SM. Investigation of the microstructure and phase transformation of microcrystalline quartz using as DVR for iron casting. *Refract. Worldforum* **2024**, *16*, 84–89. Available online: https://www.refractories-worldforum.com/issue/volume-3-2024/.(accessed on 15 August 2026)
14. *ASTM C604-18*; Standard Test Method for True Specific Gravity of Refractory Materials by Gas-Comparison Pycnometer. ASTM International: West Conshohocken, PA, USA, 2018.
15. *ISO 16835:2014*; Refractory Products—Determination of Thermal Expansion. International Organization for Standardization: Geneva, Switzerland, 2014.
16. Heaney PJ. Structure and chemistry of the low-pressure silica polymorphs. *Rev. Mineral. Geochem.* **1994**, *29*, 1–40. DOI:10.1515/9781501509698-006
17. Tian J, Zhang X, Tian Z, Mei M, Sun L, Liu X. Influencing Factors of True Density of Silica Bricks. *Eng. Test* **2014**, *54*, 52–54. DOI:10.3969/j.issn.1674-3407.2014.01.015
18. Raman CV, Nedungadi TMK. The α-β transformation of quartz. *Nature* **1940**, *145*, 147. DOI:10.1038/145147a0
19. Bale CW, Bélisle E, Chartrand P, Decterov SA, Eriksson G, Gheribi AE, et al. FactSage thermochemical software and databases, 2010–2016. *Calphad* **2016**, *54*, 35–53. DOI:10.1016/j.calphad.2016.05.002
20. Xu X, Ji G, Huang Y, Huang G, Shang B, Xu Y, et al. Research Status of Gas-Liquid Inclusion Removal Methods in High Purity Quartz. *Non-Met. Mines* **2025**, *48*, 117–123. Available online: http://www.szfjsk.com/NewsDetails-33589.html (accessed on 15 August 2026)
21. Ghiorso MS, Carmichael ISE, Moret LK. Inverted high-temperature quartz: unit cell parameters and properties of the α-β inversion. *Contrib. Mineral. Petrol.* **1979**, *68*, 307–323. DOI:10.1007/BF00371553
22. Sterner SM, Bodnar RJ. Synthetic fluid inclusions-VII. Re-equilibration of fluid inclusions in quartz during laboratory-simulated metamorphic burial and uplift. *J. Metamorph. Geol.* **1989**, *7*, 243–260. DOI:10.1111/j.1525-1314.1989.tb00587.x
23. Frezzotti ML, Tecce F, Casagli A. Raman spectroscopy for fluid inclusion analysis. *J. Geochem. Explor.* **2012**, *112*, 1–20. DOI:10.1016/j.gexplo.2011.09.009
24. Li X, Zhang Y, Han R, Wang L, Wu J, Cheng G. Research progress of fluid inclusions and its application in ore deposit. *Geol. Rev.* **2022**, *68*, 2305–2318. DOI:10.16509/j.georeview.2022.07.065
25. Fan T, Ren Z, Zhang Q, He Y, Song Y, Liu Z, et al. Quantitative Detection of Gas-Liquid Inclusions in High-Purity Quartz Sand by Double Extreme Case Analysis. *Rock Miner. Anal.* **2024**, *43*, 892–900. DOI:10.15898/j.ykcs.202410230223
26. Li Z, Tan X, Zhang L, Li J, Guo M, Liu H, et al. Utilization Characteristics and Application Progress of Quartz Resources. *Conserv. Util. Miner. Resour.* **2024**, *44*, 115–123. DOI:10.13779/j.cnki.issn1001-0076.2024.02.016
27. *YB/T 5268-2014*; Silica. Ministry of Industry and Information Technology of the People's Republic of China: Beijing, China, 2014.

28. Wang H, Cao H, Li Y. Discussion on Production and Application of High Quality Silica Brick for Glass Furnace on the Phase Transformation of Quartz. *Glass Enamel Ophthalmic Opt.* **2021**, *49*, 36–42. DOI:10.13588/j.cnki.g.e.2096-7608.2021.12.008